Agricultural and Forest Meteorology 278 (2019) 107663

Contents lists available at ScienceDirect

Agricultural and Forest Meteorology

journal homepage: www.elsevier.com/locate/agrformet

Aridity change and its correlation with greening over drylands

Bin He[a], Shuren Wang[b], Lanlan Guo[b,*], Xiuchen Wu[b]

[a] College of Global Change and Earth System Science, Beijing Normal University, Beijing 100875, China
[b] School of Geography, Beijing Normal University, Beijing 100875, China

ARTICLE INFO

Keywords:
Drylands
Aridity change
Greening
Potential evapotranspiration
NDVI

ABSTRACT

A drying trend and an expansion of drylands through history, as well as an expectation to continue under the future climate, have been inferred by recent studies. However, this seems to conflict with observed greenness over drylands. In this study, the changes in aridity over drylands from 1982 to 2011 were examined using the aridity index (ratio of precipitation and potential evapotranspiration), precipitation minus actual evapotranspiration, and soil moisture derived from a combination of observation and modelling. In addition, corresponding changes in vegetative greenness and their relationships with aridity changes were explored. The results show that above three indicators all point to a little change in aridity of drylands over the past three decades, and their trends in spatial patterns agree well each other. Simultaneously, significant greening ($p < 0.05$) occurred in more than 36% of vegetated drylands, in contrast to the 7% with significant browning ($p < 0.05$). Drylands as a whole, vegetative greenness demonstrated a significant positive relationship ($p < 0.05$) with precipitation change. At the biome scale, significant relationships ($p < 0.05$) were observed for vegetative greenness and precipitation for all other vegetation types except forests, suggesting that the increasing precipitation was one of the main drivers of greening over drylands. In addition, the largest increase of greening was observed for croplands, implying a strong impact from agricultural activities particularly irrigation practices. Results from this study provide clues for understanding the greening of drylands and are also crucial for the understanding of environmental changes in the context of climate change.

1. Introduction

Drylands occupy approximately 40% of global continents and are crucial for sustaining the world's population and regulating global carbon cycle (Huang et al., 2017a; Poulter et al., 2014). Drylands are usually defined as regions where the ratio of annual precipitation (PRE) and annual potential evapotranspiration (PET) is less than 0.65 (Huang et al., 2017a). Observation and modelling studies have suggested an expansion of global drylands, mainly driven by climate change over the past century (Feng and Fu, 2013; Sun et al., 2016), which is expected to accelerate in future climate scenarios (Huang et al., 2017b). However, controversies still exist regarding the choice of indicators of aridity (Greve et al., 2014; Milly and Dunne, 2016; Roderick et al., 2015; Swann et al., 2016; Yang et al., 2018a).

Traditionally, dryness is usually represented by indicators of difference between PRE and atmospheric water demand (Feng and Fu, 2013; Gao and Giorgi, 2008). As the measurement of evaporative demand, PET has commonly been estimated using the Penman-Monteith equation (Monteith, 1965; Penman, 1948), which reflects atmospheric water demand under well-watered condition and ignores the plant stomatal resistance term (Fisher et al., 2015; Shuttleworth, 2007). In the context of climate warming, an enhanced PET could be expected because warming induced an increasing vapour deficit (Scheff and Frierson, 2014). However, recent studies have suggested that Penman-Monteith-based PET estimates ignore the impacts of increasing CO_2 concentration on plant transpiration, leading to overestimations of output water flux, thereby overestimating drought conditions (Yang et al., 2018a). This overestimation has been confirmed by comparisons between PET and actual evapotranspiration (ET) by modelling studies. For example, Yang et al. (Yang et al., 2018b) re-examined the ET change under non-water limited condition by incorporating the changes in plant water use in response to elevating CO_2, and found that the ET increase due to climate warming has been offset by the ET decrease driven by enhanced surface resistance under rising CO_2. Swann et al. (Swann et al., 2016) evaluated and compared future drought stress with and without consideration of the influence of plant physiological responses to CO_2 concentration and found a strong overestimate of drought stress conditions when plant physiological regulation by increasing CO_2 was ignored. Similarly, Milly and Dunne (Milly and Dunne, 2016) found that Penman-Monteith PET severely over-predicts

* Corresponding author.
E-mail address: guolanlan@bnu.edu.cn (L. Guo).

https://doi.org/10.1016/j.agrformet.2019.107663
Received 17 December 2018; Received in revised form 4 July 2019; Accepted 9 July 2019

changes in ET over non-water-limited evapotranspiration regions in climate models. Hence, aridity metrics that integrate the influences of plant physiology on evapotranspiration have been recommended for dryness measurements, such as PRE-ET, soil moisture, runoff, and land water storage (Berg and Sheffield, 2018; Roderick et al., 2015; Swann et al., 2016). However, the use of these metrics for long-term dryness assessment has been limited by a lack of observations.

Greening over some parts of drylands since the 1980s has been reported by an increasing number of studies (Donohue et al., 2013; Fensholt et al., 2012; Hickler et al., 2005; Poulter et al., 2014). This apparently contradicts the idea that drylands are drying, because available water conditions are the main constraint on vegetation growth in drylands (Nemani et al., 2003). Hence, this study investigated aridity trends over drylands from 1982 to 2011 using both atmospheric-based and plant-based dryness indicators and explored the changes and drivers of vegetation greenness over drylands. The atmospheric-based indicator is represented by the commonly used aridity index (AI), defined as the ratio of PRE to PET (Gao and Giorgi, 2008; Huang et al., 2017b). The plant-based dryness indicators used here include the difference among PRE and ET (Greve et al., 2014; Swann et al., 2016) and soil moisture (SM).

2. Data and methodology

2.1. Data

To ensure that the results are independent of the data sets used, for each dryness indicator, multiple sources of data sets were used for the calculation of each dryness indicator, including four PRE data sets, five PET data sets, three ET data sets, one SM data set and one NDVI product. Detailed information for all data sets used in this study are listed in Table 1. All PET data sets were calculated based on the Penman-Monteith method (Penman, 1948), which has been recognized as a physical-based approach by comprehensively accounting for influences from temperature, solar radiation, wind speed, humidity, etc. (McVicar et al., 2012). These data sets comprised a total of 20 PRE/PET combinations and 12 PRE-ET combinations.

In addition, a recent study has suggested that the Penman-Monteith method ignores the effect of rising CO_2 on surface resistance (r_s) (Yang et al., 2018a), and thereby overestimates the PET. Hence, in this study, we also calculate the PET by incorporating influence from changes of surface resistance under elevating CO_2. The detailed description on the calculation method can be found in Yang et al.'s (Yang et al., 2018a) study.

2.2. Methodology

2.2.1. Aridity index (AI)

The aridity index (AI) is defined as the ratio of the annual P to the annual PET (Feng and Fu, 2013) and represents the degree of climatic aridity in a region. Drylands are confined to regions with AI < 0.65 and are further divided into dry subhumid ($0.5 \leq AI < 0.65$), semi-arid ($0.2 \leq AI < 0.5$), arid ($0.05 \leq AI < 0.2$) and hyper-arid ($AI < 0.05$) regions (Gao and Giorgi, 2008). Fig. S1 shows the spatial distribution of global drylands. It was drawn according to the AI index, which was calculated from 20 combinations of P and PET from 1982 to 2011.

2.2.2. PRE-ET

According to recommendations of previous studies (Greve et al., 2014; Swann et al., 2016), the difference between PRE and ET, defined as PRE-ET, was used to indicate the changes in surface water availability. This index was considered to include the influences of plant physiological regulation by CO_2 concentration on surface water availability on land (Swann et al., 2016). Two observation-based ET products and one modelling-based ET product were used here. The ET product provided by Zeng et al. (Zeng et al., 2012, 2014) was estimated using the water balance equation based on observations of runoff, precipitation and terrestrial water storage changes retrieved from the Gravity Recovery and Climate Experiment (GRACE) satellites. Another observation-based ET product was developed by Jung et al. (Jung et al., 2010) using up-scaling station measurements of eddy-covariance fluxes from the global FLUXNET database with a machine learning algorithm. A series of ET products simulated by land surface models can be freely obtained. Here, we selected the product simulated by the Global Land Evaporation Amsterdam Model (GLEAM) because it incorporates satellite observations, and it has been proved to be relatively reliable and has been widely used in studies of land-atmosphere interactions (Martens et al., 2017; Miralles et al., 2011, 2014).

2.2.3. Soil moisture

SM is the water content stored at a given layer of soil. Due to the scarcity of *in situ* observations, large scale investigations still rely on satellite retrievals or model simulations. Here, the root-zone SM simulated by the Global Land Evaporation Amsterdam Model (GLEAM) was used. This SM product is calculated using a multi-layer running-water balance model forcing by net precipitation and snowmelt. The depth of

Table 1
Datasets used in this study.

Variables	Product	Temporal Resolution	Spatial Resolution	Periods
TEM	Climate Research Unit (CRU)	monthly	0.5°	1982–2011
PRE	Climate Research Unit (CRU)	monthly	0.5°	1982–2011
	Global Precipitation Climatology Center (GPCC)	monthly	0.5°	1982–2011
	Climate Prediction Center (CPC)	daily	0.5°	1982–2011
	University of Delaware (UD)	monthly	0.5°	1982–2009
PET	Climate Research Unit (CRU)	monthly	0.5°	1982–2011
	Four other PET datasets provided by Feng and Fu (Feng and Fu, 2013)	monthly	0.5°	1982–2009
ET	Provided by Zeng et al. (Zeng et al., 2012, 2014)	monthly	0.5°	1982–2011
	Provided by Jung et al. (Jung et al., 2010)	daily	0.5°	1982–2011
	Global Land Evaporation Amsterdam Model (GLEAM) Version 3.2 datasets (Martens et al., 2017; Miralles et al., 2011)	daily	Original: 0.25°, interpolate to 0.5°	1982–2011
NDVI	Global Inventory Monitoring and Modelling Systems (GIMMS) 3 g	daily	Original: 0.083°, interpolate to 0.5°	1982–2011
SM	Global Land Evaporation Amsterdam Model (GLEAM)	daily	Original: 0.25°, interpolate to 0.5°	1982–2011
	European Space Agency (ESA)	daily	Original: 0.25°, interpolate to 0.5°	1982–2011
Land cover	Moderate-resolution imaging spectroradiometer (MODIS)	yearly	500 m	2012
Irrigation area	Food and Agriculture Organization of the United Nations (FAO)[a]	5 minutes	8km	2013

[a] Irrigation data is from: www.fao.org/nr/water/aquastat/irrigationmap/index10.stm.

plant root zone is defined using a function of land cover types, and ranges from 0 to 250 cm. To reduce simulation errors, a satellite SM product, the ESA SM, is blended from both passive and active microwave soil moisture retrievals from various satellites and is assimilated into the GLEAM SM. Therefore, the GLEAM SM product is a combination of observation and simulation and is widely used in studies of land surface processes (Guillod et al., 2015; Miralles et al., 2014).

2.2.4. Statistical analysis

Two statistical analysis methods were used to assist our analysis, the Pearson's correlation analysis (Benesty et al., 2009) and the Mann-Kendall (MK) test (Kendall, 1955; Mann, 1945), which were used to explore relationships and trends in the studied variables, respectively. The significances of correlations and trends were both assessed at $p < 0.05$.

3. Results

3.1. Climate change over drylands during 1982–2011

We first examined changes in climatic conditions over drylands. The linear trends in temperature (TEM), PRE, PET and ET over drylands from 1982 to 2011 are shown in Fig. 1. For drylands as a whole, the annual mean PRE is 323.74 mm during 1982 to 2011. PRE presents a significant increase ($p < 0.05$) trend despite large interannual variations. It has increased by 18.63 mm over the past three decades. The annual mean TEM over drylands is 13.82 ℃. It also demonstrates a significant ($p < 0.05$) increase trend, and has increased by 1.065 ℃ during the study period.

Estimated using the PM algorithm, the multi-year mean PET is 1424.15 mm/yr, which has increased at a rate of 1.44 mm/yr over the past three decades. We observed a high coincidence of changes in PET with TEM ($R = 0.624$, $P < 0.01$) (Table S1). This is because that the increased TEM will promote the vapour pressure deficit (VPD) and thus the atmospheric water demand. As the PM based PET estimation holds the surface resistance as a fixed term, then a VPD increase caused PET rising could be expected as reported by previous findings (Feng and Fu, 2013; Scheff and Frierson, 2014).

An average 299.10 mm/yr ET over drylands was estimated based on 3 products and shows a significant increase ($p < 0.05$) from 1982-2011. Different from PET driven by TEM, the variation in ET seems to be forced by PRE. Correlation analysis suggests that there is a significant relationship between PRE and ET ($R = 0.903$, $P < 0.01$) (Table S1). This is not surprising because drylands are mainly water-limited ET regions (McVicar et al., 2012; Wang and Dickinson, 2012). Although both PRE and ET show positive trends, the slope of the former is higher than that of the latter. The total increase in ET over the past three decades is 15.66 ± 7.60 mm, which is smaller than PRE (19.63 ± 13.03 mm).

Fig. 2 shows the trends of the above four variables spatially. We can clearly see a high correlation in the patterns of TEM and PET. The majority of drylands (87%) experienced significant warming ($p < 0.05$) over the past three decades, which likely drives the increase in PET. Simultaneously, a similar pattern was also observed between PRE and ET. From 1982 to 2011, approximately 14% of drylands experienced significant increases ($p < 0.05$) in PRE, mainly occurring in North and South Africa, west China and North Australia, which also experienced increases in ET. In contrast, significant decreases ($p < 0.05$) in PRE were observed over 7% of drylands, such as in northern America, the Sinai Peninsula, and northeast China, which were usually associated with decreases in ET.

3.2. Dryness change indicated by AI over drylands from 1982 to 2011

AI calculated from 20 combinations of PRE and PET showed a weak increasing trend over the past three decades (Fig. 1), implying a wetting tendency over drylands. We observed a significant relationship between AI and PRE ($R = 0.875$, $P < 0.01$), but a weak negative relationship between AI and TEM (Table S1). Spatially, the distribution of AI trends agrees well with the pattern of PRE trends but not with the pattern of TEM trends (Fig. 2). A total of 11% of drylands showed significant wetting ($p < 0.05$), in contrast to 8.4% that showed significant drying

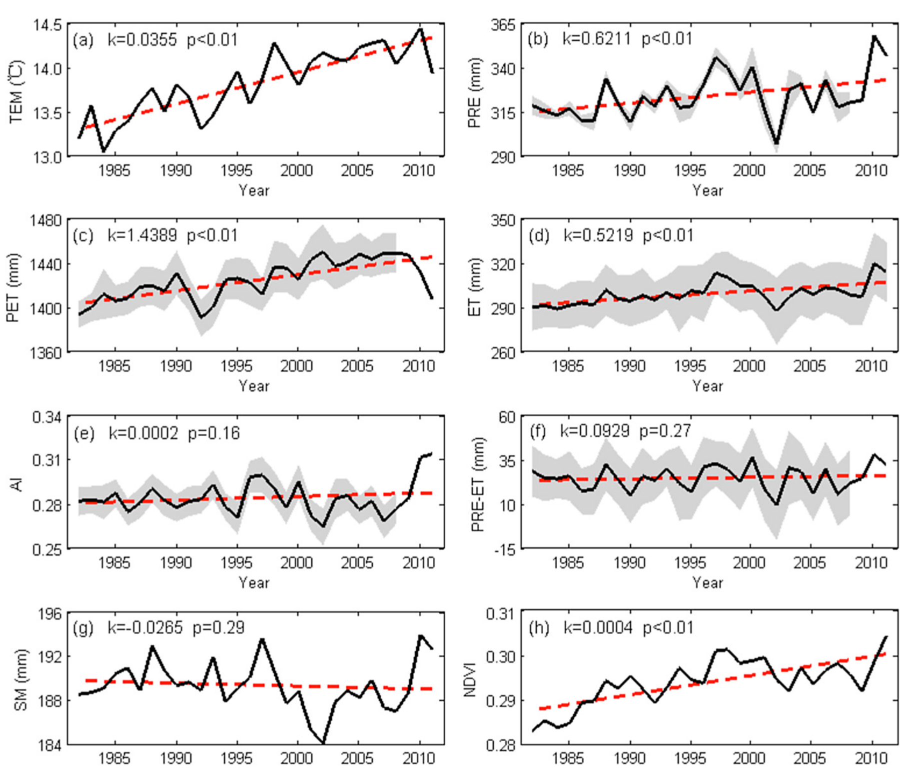

Fig. 1. Interannual variations in TEM, PRE, PET, ET, AI, PRE-ET, SM and NDVI over drylands from 1982 to 2011 (a–h). The solid line indicates the mean value of multiple datasets, and the shaded area indicates the standard deviation of multiple datasets. The red broken line illustrates the linear trend for the curve. The k and p denote the slope and p-value of the trend of the red broken line, respectively.

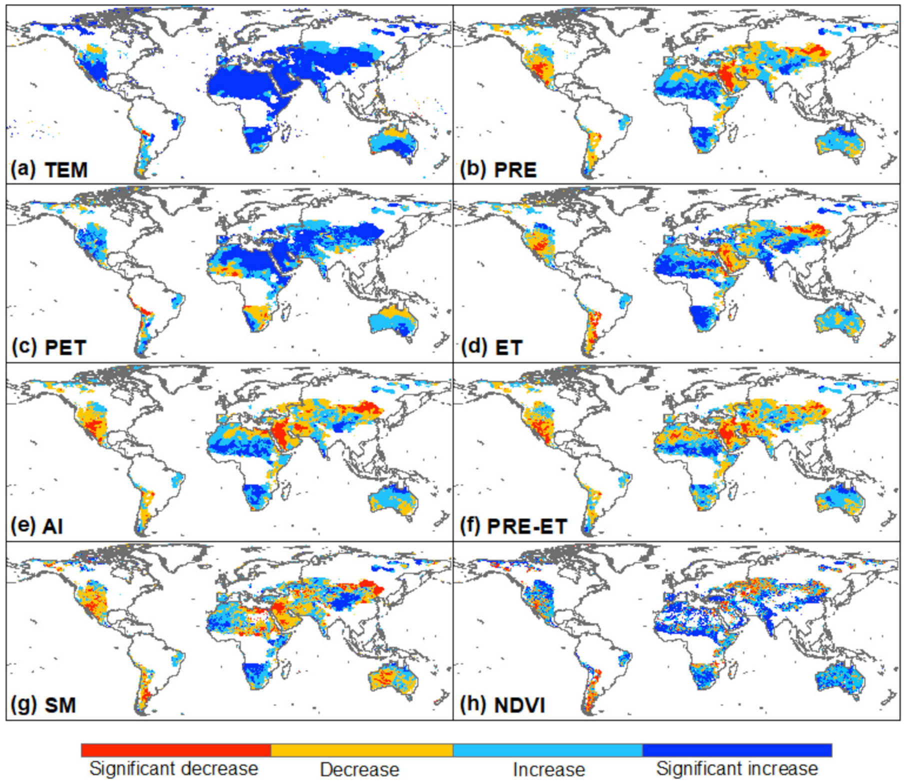

Fig. 2. Spatial distributions of trends in TEM, PRE, PET, ET, AI, P-ET, SM and NDVI (a–h) over drylands from 1982 to 2011.

($p < 0.05$). Climate wetting occurred in drylands in north-western China, India, Africa, north Australia and eastern South America, etc. In contrast, climate drying was observed in drylands in the Mongolia Plateau, west Asia, southern North America and southern South America.

Simultaneously, the area ratio of drylands calculated from annual AI < 0.65 presents a significant decreasing trend ($p < 0.05$) (Fig. S2), implying a reduction of drylands. Total drylands decreased by 1.52% over the past three decades. To understand the changes in drylands over the last 30 years, we divided the entire study period into two periods, the first 15 years (from 1982 to 1996) and the most recent 15 years (from 1997 to 2011), and investigated changes in dryland areas. Fig. S3 and Table S2 show the transformation between different categories of drylands for 1997–2011 relative to 1982–1996. We observed comparable area ratios between those that shifted to a drier class compared to those that shifted to a wetter class, 2.69% *vs.* 3.11%. The expansions of drying, such as arid to hyper-arid or semiarid to arid, mainly occur in North America, central and west Asia and southern Australia. On the other hand, expansions of wetting like hyper-arid to arid or arid to semiarid mainly occur in southern South America, central and southern Africa and northern Australia.

3.3. Dryness change indicated by surface water balance (PRE-ET) over drylands from 1982 to 2011

The average PRE-ET from 1982 to 2011 was 25 mm/yr. The annual P-ET shows great interannual variation with a minimum value of 9 mm/yr and a maximum value of 38 mm/yr. For drylands as a whole, PRE-ET shows a weak increase over the past three decades (Fig. 1), which suggested a promoted water yield over drylands. It was found to be more correlated to PRE ($R = 0.924$, $P < 0.01$) than ET ($R = 0.670$, $P < 0.01$) (Table S2). In addition, a significant positive relationship was observed between PRE-ET and AI ($R = 0.859$, $P < 0.01$). The spatial pattern of PRE-ET trends is also roughly consistent with PRE and AI, but seems to be smaller in slope than PRE and AI. Significant positive/negative trends ($p < 0.05$) were observed over 8% and 7% of drylands. Significant decreasing trends ($p < 0.05$) mainly occurred in south western North America and west Asia; significant increasing trends ($p < 0.05$) mainly occurred in northern Australia and central and southern Africa.

3.4. Dryness indicated by SM

The average SM from 1982 to 2011 was 189 mm. It showed a weak decreasing trend with a slope of -0.0265 mm/yr over the past three decades. The interannual variation of regional averaged SM demonstrated high coherency among PRE ($R = 0.829$, $P < 0.01$), ET ($R = 0.825$, $P < 0.01$), AI ($R = 0.824$, $P < 0.01$) and PRE-ET ($R = 0.694$, $P < 0.01$) (Table S1). This high coherency is also reflected in the spatial pattern of the SM trend with trends of these variables (Fig. S4). The area ratios of drylands with a coherency trend between SM and PRE, AI, PRE-ET, SM are 85.03%, 84.83%, 74.66% and 88.18% of drylands, respectively, suggesting that the simulated SM can basically capture drying and wetting trends.

3.5. Vegetation change and its relationship with dryness indicators

Vegetation changes can reflect environmental changes over drylands, especially water availability conditions. The average NDVI shows a strong increasing trend over the past three decades (Fig. 1), which is consistent with widely reported greening over Africa (Dardel et al., 2014), Australia (Donohue et al., 2009; Yang, 2014), south Asia (Wang et al., 2017), etc. Significant greening ($p < 0.05$) is observed in 36% of drylands (Fig. 2). Vegetation browning is mainly found in West Asia and southern South America, accounting for 7% of total drylands.

The interannual variations in NDVI for each vegetation type were also examined. Except for forests, all vegetation types show a significant increasing ($p < 0.05$) trend. The largest increase in NDVI occurred in croplands, which accounted for 11.87% of global drylands, implying strong influences from agricultural practices on vegetation growth.

Savannas mainly concentrated in Africa, Australia and South America account for 8.37% of total drylands. The overall NDVI of savannas presents a secondary increasing rate. Shrublands and grasslands have comparable area ratios, approximately 22% but have different distribution patterns. Shrublands are mainly located in the Southern Hemisphere, and grasslands are mainly distributed in the Northern Hemisphere. In addition, the NDVI of the shrublands demonstrates a larger increasing rate than that of the grasslands. Barren vegetated areas are mainly located in Africa and Asia, accounting for the largest proportion of dryland; their overall NDVI also shows an increasing trend. Forests only account for 2.51% of total drylands, and are mainly distributed in central South America and parts of northern Asia. Forests in drylands usually grow near rivers and are mainly affected by changes in groundwater (Cunningham et al., 2011), or by meltwater from ice and snow (Jarvis, 2000), so the relationship between NDVI and PRE in forests in insignificant.

Water availability is the main constraint of vegetation growth in drylands. Hence, the relationships among NDVI and PRE, AI, PRE-ET and SM were examined (Table S1). The regional mean NDVI over vegetated drylands (excluding barren lands) shows the highest correlation with PRE ($R = 0.423$, $P < 0.05$), followed by SM ($R = 0.348$, $P > 0.05$), AI ($R = 0.\ 252$, $P > 0.05$) and PRE-ET ($R = 0.\ 167$, $P > 0.05$). Spatially, vegetation growth positively responds to dryness indicators over the majority of drylands, and areas with significant relationships ($p < 0.05$) (positive) accounted for 39.29%, 38.79%, 19.73%, and 41.11% of vegetated drylands (Fig. S5). PRE-ET presented a relatively weak relationship with NDVI compared to the other three indicators. The reason may be that ET includes water used by plants, and PRE-ET truly reflects the surface runoff. At the biome scale, except for forests, significant positive relationships ($p < 0.05$) between NDVI and PRE are observed for all vegetation types, as shown in Fig. 3. In addition, except for forests and barelands, increasing PRE and associated enhancing NDVI occur in all other four types, suggesting a potential promotion of PRE on vegetation greenness.

Greening over drylands as observed here has been reported by previous studies (Fensholt et al., 2012; Ulf Helldén, 2008; Yang et al., 2015; Zhu et al., 2016). Explanations for this greening include increasing precipitation and associated moisture conditions (Hickler et al., 2005), increasing plant use efficiency of rainfall (Dardel et al., 2014), and the CO_2 fertilization effect (Donohue, 2017; Donohue et al., 2013; Lu et al., 2016). Here, we also observed extensive greening over drylands (Fig. 2). The above analysis suggests a close relationship between NDVI and PRE at both regional and biomes scales. In addition, 60.22% of drylands experienced PRE increases, among which 86.30% happened in vegetated areas, in contrast to 13.70% in barelands, imply that increasing PRE-related water availability is still one of the main drivers of greening in drylands. On the other hand, about 69.70% of areas those featured with significant greening experienced PRE increases, suggesting a PRE increase can only explain part of greening over drylands. Human-associated activities, especially agricultural practices such as irrigation, fertilization, etc., may also contribute to greening, based on an observed strong increase in the greenness of croplands. This can be further supported by the global irrigation map (Fig. S6). Statistics shows that 21.44% of drylands are equipped with irrigation facilities, and 30.99% of significant greening ($p < 0.05$) areas are influenced by irrigation. A high irrigation ratio can be clearly found in western USA, Arab regions and north-eastern parts of China where experienced decreases in PRE, but increases in NDVI.

3.6. Dryness and vegetation change over different continents

All of the drylands were divided into different continents and biome types, and their corresponding trends for PRE, AI, PRE-ET and SM were further examined (Fig. 4). At the continental scale, Africa is mainly covered by bare areas, forests and savannas. NDVI values for all vegetation types showed increasing trends, and the largest increases were observed for croplands. Accompanying widespread greenness, more than four dryness indicators consistently suggest a wetting trend over drylands in Africa, implying a wetting-stimulated greening, as has been reported by previous investigations (Dardel et al., 2014; Hickler et al.,

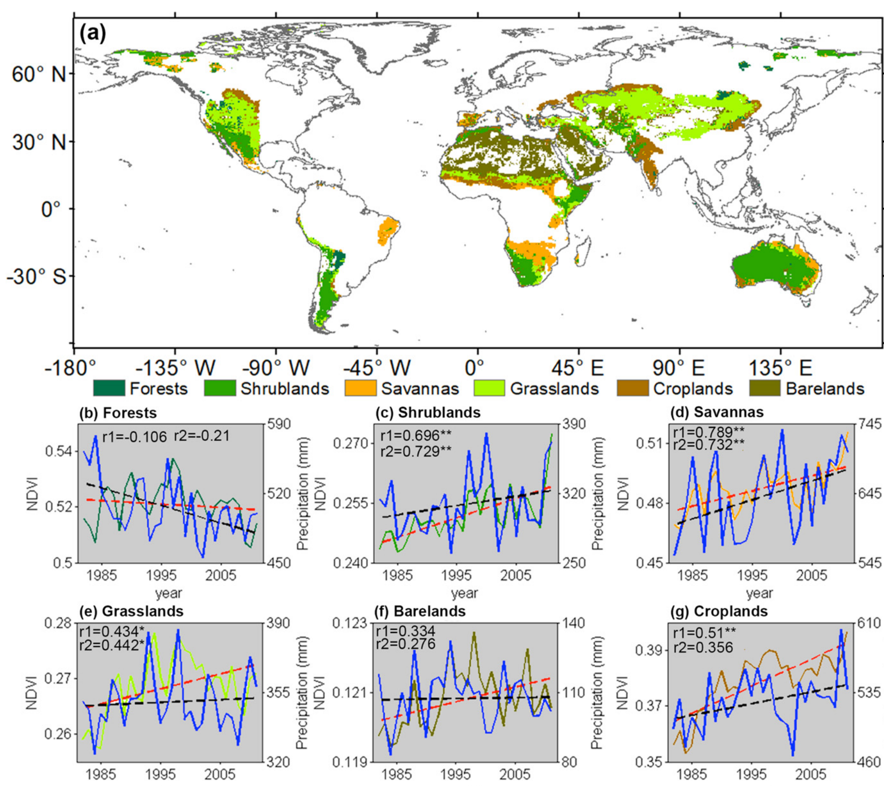

Fig. 3. Land cover of dryland (a) and interannual variation in NDVI for different vegetation types and its relationship with precipitation (b–g). In each polyline map, the blue solid line and another colour solid indicate the interannual variation of PRE and NDVI for each land cover type, respectively; the red and black dashed lines illustrate the linear trends for the NDVI and PRE, respectively. The line colours of NDVI for different land cover types are consistent with those used in the above land cover map. The r1 and r2 in (b–g) are the correlation coefficients between NDVI and PRE determined using the original and detrended time series, respectively. * indicates a significant correlation between NDVI and PRE with $P < 0.05$, and ** indicates a strong significant correlation between NDVI and PRE with $P < 0.01$.

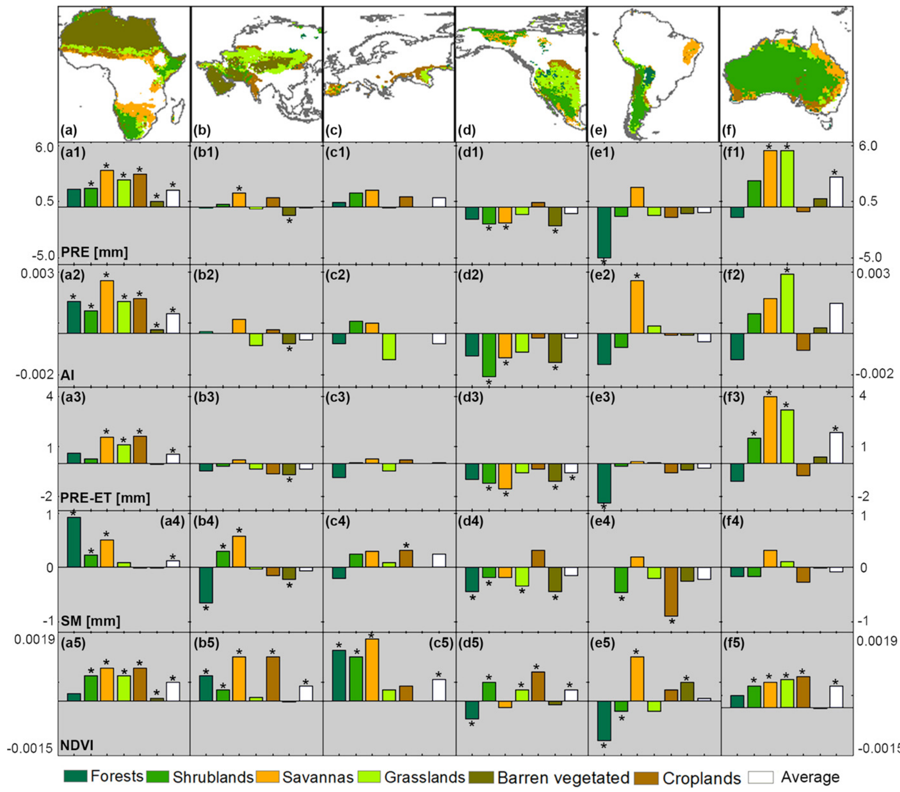

Fig. 4. Land cover types of different continents (a–f) and the trends of PRE (a1 - f1), AI (a2 - f2), PRE-ET (a3 - f3), SM (a4 - f4) and NDVI (a5 - f5) for different continents. * indicates a significant variation with $P < 0.05$, and ** indicates a strong significant variation with $P < 0.01$.

2005).

In the drylands of Asia, all four dryness indicators suggest a weak drying trend, but the vegetation still shows significant increases ($P < 0.05$). The savannas show the largest increases, which seems to be promoted by the increases in moisture conditions. We also observed a large increase in the NDVI of croplands, implying potential influences of human activities. Except for bare lands, grasslands are the main vegetation type in Asia's drylands. The overall NDVI of grasslands demonstrate an increasing trend despite the weak decrease in moisture conditions. Several reasons can explain the enhanced growth of grass, including regional wetting (e.g., West China) (Peng and Zhou, 2017), moisture increases caused by warming-induced snowmelt in surrounding mountainous areas (Ren et al., 2007), and regional ecological protection practices (e.g., North China) (Lü et al., 2015).

Drylands distributed in Europe only account for 2.74% of global drylands, and about half are covered by croplands. This may be the main reason for the largest vegetation increases compared to those of the other continents. Except for PRE, the other three indicators indicate wetting. Therefore, increased vegetation growth on this continent may be attributed to improved moisture conditions and agricultural practices.

The drylands in North America experienced apparent drying, as reflected by all four indicators. However, we still observed increases in NDVI. The largest increases in vegetation growth occurred in croplands, which can be explained by irrigation activities (Mueller et al., 2016). This is also supported by increases in SM. In comparison to Fig. S6, we find those areas featured as grasslands are also heavily irrigated areas. Hence, we speculate the significant NDVI increase ($p < 0.05$) over grasslands should also be attributed to the irrigation activities. Significant increase in NDVI occurred over shrublands which are mainly concentrated in the south-western United States. However, contrasting trends in four dryness indicators were observed. In light of previous investigations, spring-summer snowmelt is critical for vegetation growth in this areas (Notaro, 2010), particularly for shrubs which are mainly maintained by deep soil water (Kurc, 2010). The increase NDVI is likely stimulated by increasing deep soil water accumulations caused by warming associated snowmelt. This can be supported by the significant correlation between NDVI and TEM ($R = 0.45$, $p < 0.05$) observed in this study. The above analysis suggests that both human activities and climate change contribute to the increase of average NDVI in the drylands of North America.

A relatively high coherency trend of NDVI and dryness indicators occurred in the drylands of South America. All four dryness indicators point to a drying trend, but the average NDVI still shows a weak increase which seems to be contributed from the NDVI increase in savannas in the east. The large increase of NDVI in savannas is associated with increases in all for four dryness indicators, suggesting a wetting driven greening. The NDVI increase is also observed in croplands, and should be stimulated by irrigation practices (Fig. S6) because dryness indicators all suggest a drying trend. A drying related NDVI decrease occurs in forests, shrublands and grasslands, implying a risk of ecosystem degradation.

The majority of Australia is drylands, where PRE, AI and PRE-ET all demonstrate an increasing trend, whereas SM presents a weak decrease. In the meantime, all types of vegetation demonstrate an increasing trend, especially for croplands where irrigation activities are observed (Fig. S6). We speculate that the overall greening of Australia's drylands can be explained by increasing moisture conditions. Without considering the uncertainties of SM datasets, a potential explanation for the overall decrease in SM is that increasing vegetation growth decreases SM through evapotranspiration.

4. Discussion and conclusions

By using a metric of aridity indices including climate-based and plant-based indices, this study examined changes in aridity over drylands from 1982 to 2011. Drylands experienced increases both in temperature and precipitation, which affected the PET and ET,

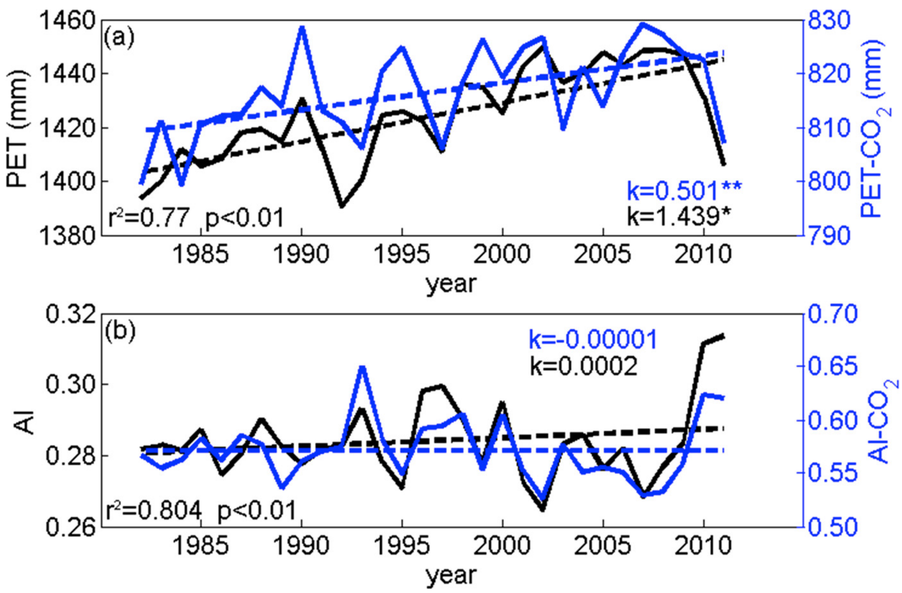

Fig. 5. Interannual variations of PET and AI with and without considering the response of surface resistance to rising CO_2 during 1982–2011 (a – b). In each polyline map, the black and blue solid lines indicate the interannual variation of PET/AI with and without considering the response of surface resistance to rising CO_2, respectively; the black and blue dashed lines illustrate the linear trends for the black and blue solid lines, respectively.

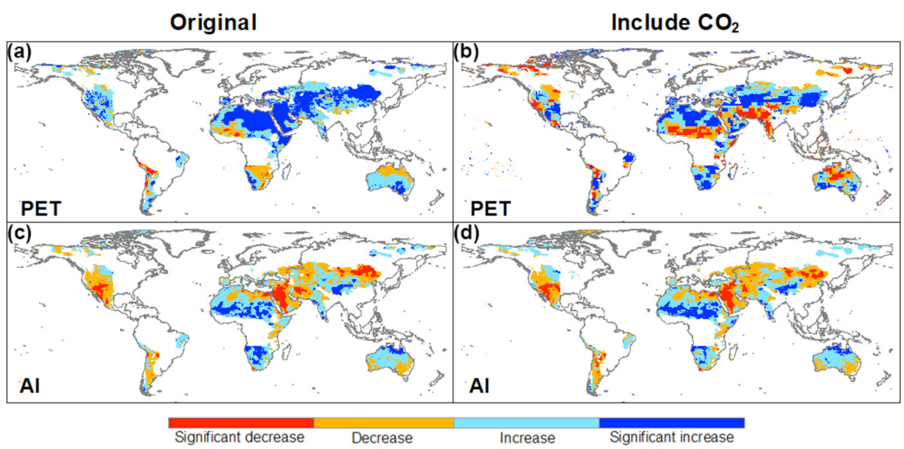

Fig. 6. Spatial distributions of trends in PET and AI with and without considering the response of surface resistance to rising CO_2 during 1982–2011 (a–d).

respectively. This is reasonable because the warming-induced increases in atmospheric water demand has been thoroughly discussed in previous studies (Berg et al., 2016; Feng and Fu, 2013; Scheff and Frierson, 2014). Furthermore, in drylands, ET is mainly constrained by water supply conditions (Jung et al., 2010). We observed few changes in the dry/wet conditions of drylands, as indicated by AI, PRE-ET and SM over the past three decades. Despite the strong increase in T, which greatly promoted PET, its influence on AI was counter-acted by an increase in P and ultimately produced a weak increase in AI. A recent study suggests that the ignoring of the rising CO_2 on surface resistance would overestimate the PET. In line with Yang et al.'s method (Yang et al., 2018a), we re-calculate the PET and AI by incorporating the influence of elevating levels of CO_2, as shown in Figs. 5 and 6 . Compared to original PET, the newly generated PET presents a similar but lower rising rate when considering the response of surface resistance to rising levels of CO_2. Accordingly, the newly generated AI demonstrates a weak decreasing trend in contrast to the weak increasing trend of the original AI, suggesting a wetting climate over drylands. Spatially, we observe a more extent decrease in newly generated PET than the trend pattern of original PET especially in the north of Africa, the southwest of Asia, the north of Northern America etc. Despite the different patterns in two PET trends, the spatial distribution of newly generating AI presents a relatively consistent pattern with that of the original AI, but the former has more wetting areas and less drying areas than the later. The above analysis suggests that ignoring the impact of rising CO_2 on surface resistance would truly overestimate the PET and thus overestimate the drying trend over drylands.

In drylands, ET is controlled by water supply conditions (McVicar et al., 2012). As the main surface water input, the PRE increase also promotes the ET. P-ET demonstrates a weak increase, implying an enhancing surface water yield. Previous investigations have suggested that increasing CO_2 concentrations may promote plant water use efficiency (Lu et al., 2016; Swann et al., 2016). If this stands, an increase in PRE-ET is theoretically expected. However, the effect of CO_2 concentrations on plant water use efficiency is still controversial (Tan, 2015; Yan, 2014). In contrast to the increasing trend of AI and P-ET, SM presented a weak decreasing trend. Ignoring the potential uncertainties of the SM dataset, a possible explanation is that enhanced vegetation growth dries the SM (Wolf et al., 2016). It should be noted that croplands account for 11.87% of total drylands, implying a potential influence by human activities in our results. Hence, all indicators were recalculated excluding croplands, as shown in Fig. S7. By comparing the results to Fig. 1, we found that there was no apparent difference in the overall trends in aridity indictors between the two conditions, suggesting little influence of agricultural activities on the drying and wetting patterns of drylands. However, a difference in the slopes of indicators between the two conditions was observed. In particular, we found an apparent decrease in the slope of NDVI, implying the potential influence of agricultural practices on dryland greening. The few change of aridity concluded from this study seems to conflict with previous reports that claim a climate drying of drylands (Feng and Fu, 2013). This difference may be caused by selecting a different aridity indicator, study period, and data sets.

On the continental scale, dry/wet changes exhibit great spatial differences over drylands. Apparent wetting of drylands occurred in Africa, Australia and central and southwest Asia. Improved water availability seems to promote vegetation growth, as has been reported by previous investigations (Dardel et al., 2014; Donohue et al., 2009; Wang et al., 2017). In contrast, obvious drying of drylands was observed in North and South America as well as East and West Asia, and apparent decreases in soil moisture decreased vegetation growth in South America. For drylands as a whole, more than 70% of vegetated drylands demonstrated a coherent trend between NDVI and P over the study region, suggesting a strong impact of water availability on vegetation growth. At the biome scale, except for forests, the NDVI of other main vegetation types all show significant increasing trends ($p < 0.05$) and were also significantly ($p < 0.05$) correlated with changes in PRE, implying that the observed greening seems to be mainly attributed to the increase in PRE, as has been reported in Sahel (Hickler et al., 2005). We further explored the changes in NDVI and corresponding aridity indicators in each sub-region of drylands, as shown in Fig. S8. We clearly see that except for hyper-arid regions, the other three regions all experienced increases in PRE associated with increases in AI and PRE-ET, implying a wetting trend for these regions even though increasing SM was only observed in semiarid regions. The plants in the four regions all exhibited increasing greenness, and the largest increase occurred in the semiarid region. Considering the few plants in hyper-arid regions accounting for 14.52% of total drylands, we concluded that greening over drylands was strongly stimulated by improved water availability. This finding seems to reconcile the conflict between drying and greening over drylands because drying mainly occurred in hyper-arid regions with barren lands; in contrast, other drylands experienced increasing PRE and greening. In addition, irrigation plays an important role in sustaining agricultural and livestock production in dryland (A, 2016; Bestelmeyer, 2015), and would inevitably influence the vegetation change. We find about one-third of significant greening ($p < 0.05$) areas have irrigation practices, implying a great stimulation of irrigation on drylands greening. Chen et al's study (Chen, 2019) also reveals a rapid increase of cropland irrigation over drylands, and suggests that a human-induced increase in crop canopy cover is a main driver of irrigation increases. This study simply analysed the drylands greening from the perspective of aridity change, other reasons that may also contribute the greening such as land-use change (Bestelmeyer, 2015), the CO_2 fertilization effect (Donohue et al., 2013; Lu et al., 2016), grazing activities (Bestelmeyer, 2015), shrub encroachment (Turnbull, 2019) etc., still need in-depth study in the future.

Using multiple lines of evidence, this study suggests a slight change in dryness over drylands from 1981 to 2011. The increased greenness over drylands is likely triggered by improved water availability associated with increased precipitation and improved irrigation. In addition, irrigation practices seem to also contribute to greening at the local scale. Findings from this study are crucial for understanding the impacts of climate change on environmental changes in the drylands. However, uncertainties remain. First, uncertainties occur with the datasets used here. The meteorology stations were sparsely distributed over drylands. This strongly influences the accuracy of gridded climate products that are constructed based on observations from meteorology stations. In addition, uncertainties in ET datasets, SM datasets and the NDVI dataset cannot be ignored. Second, PET is a key variable for determining dryness conditions. It is driven by both energy and aerodynamic components. Due to the lack of observations (e.g., wind speed), influences from all these components were not thoroughly considered in this study. Third, the relative contributions of climate change and human activities to dryland greening have not been well quantified. This should be further addressed with ecological modelling.

Acknowledgements

Special thanks for Scott Welsh for helping us to polish the language of our manuscript, and thanks for S. Feng and J.P. Huang for providing us the PET data. This work is financially supported by the National Key Research and Development Program of China (Grant no. 2017YFA0603601 & 2016YFC0500805), the Strategic Priority Research Program of Chinese Academy of Sciences (Grant No. XDA20060402) and the National Natural Science Foundation of China (Grant No. 41101074, 41671083, 41201261 and 41730639). We thank S. Feng and J.P. Huang for providing us the PET data. The GIMMS NDVI3g data set was obtained from https://ecocast.arc.nasa.gov/data/pub/gimms/. Global P data was obtained from the Climatic Research Unit (CRU) Time Series 4.01, the Global Precipitation Climatology Center (GPCC), the Climate Prediction Center (CPC) and the University of Delaware (UD), respectively. Global T and PET data was both obtained from the CRU Time Series 4.01. Global SMroot data was collected from the Global Land Evaporation Amsterdam Model (GLEAM) version 3.1 datasets. Global ET products were obtained from GLEAM version 3.1 datasets, Zeng et al. (Zeng et al., 2012; Zeng et al., 2014) and Jung et al. (Jung et al., 2010), respectively. Global land cover map was extracted from Moderate-resolution imaging spectroradiometer (MODIS) land cover product (MCD12Q1).

Appendix A. Supplementary data

Supplementary material related to this article can be found, in the online version, at doi:https://doi.org/10.1016/j.agrformet.2019.107663.

References

A, T., 2016. Rethinking the sustainability of Israel's irrigation practices in the Drylands. Water Res. 90, 387–394.
Benesty, J., Chen, J., Huang, Y., Cohen, I., 2009. Pearson Correlation Coefficient, Noise Reduction in Speech Processing. Springer, pp. 1–4.
Berg, A., et al., 2016. Land-atmosphere feedbacks amplify aridity increase over land under global warming. Nat. Clim. Chang. 6 (9).
Berg, A., Sheffield, J., 2018. Climate change and drought: the soil moisture perspective. Curr. Clim. Change Rep. 4 (2), 180–191.
Bestelmeyer, B.T., O.G.S, Duniway, M.C., et al., 2015. Desertification, land use, and the transformation of global drylands. Front. Ecol. Environ. 13 (1), 28–36.
Chen, Y., F.X, Fu, B., et al., 2019. Recent global cropland water consumption constrained by observations. Water Resour. Res. 55 (5), 3708–3738.
Cunningham, S.C., Thomson, J.R., Mac Nally, R., Read, J., Baker, P.J., 2011. Groundwater change forecasts widespread forest dieback across an extensive floodplain system. Freshw. Biol. 56 (8), 1494–1508.
Dardel, C., et al., 2014. Re-greening Sahel: 30 years of remote sensing data and field observations (Mali, Niger). Remote Sens. Environ. 140, 350–364.
Donohue, R.J., R.M.L, Mcvicar, T.R., et al., 2017. A simple hypothesis of how leaf and canopy-level transpiration and assimilation respond to elevated CO2 reveals distinct response patterns between disturbed and undisturbed vegetation. J. Geophys. Res. 122 (1), 168–184.
Donohue, R.J., McVICAR, T.R., Roderick, M.L., 2009. Climate-related trends in Australian vegetation cover as inferred from satellite observations, 1981–2006. Glob. Chang. Biol. 15 (4), 1025–1039.
Donohue, R.J., Roderick, M.L., McVicar, T.R., Farquhar, G.D., 2013. Impact of CO_2 fertilization on maximum foliage cover across the globe's warm, arid environments. Geophys. Res. Lett. 40 (12), 3031–3035.
Feng, S., Fu, Q., 2013. Expansion of global drylands under a warming climate. Atmos. Chem. Phys. 13 (19), 10081–10094.
Fensholt, R., et al., 2012. Greenness in semi-arid areas across the globe 1981–2007 — an Earth observing satellite based analysis of trends and drivers. Remote Sens. Environ. 121, 144–158.
Fisher, J.B., Whittaker, R.J., Malhi, Y., 2015. ET come home: potential evapotranspiration in geographical ecology. Glob. Ecol. Biogeogr. 20 (1), 1–18.
Gao, X., Giorgi, F., 2008. Increased aridity in the Mediterranean region under greenhouse gas forcing estimated from high resolution simulations with a regional climate model. Glob. Planet. Change 62 (3), 195–209.
Greve, P., et al., 2014. Corrigendum: global assessment of trends in wetting and drying over land. Nat. Geosci. 7 (10), 848.
Guillod, B.P., Orlowsky, B., Miralles, D.G., Teuling, A.J., Seneviratne, S.I., 2015. Reconciling spatial and temporal soil moisture effects on afternoon rainfall. Nat. Commun. 6, 6443.
Hickler, T., et al., 2005. Precipitation controls Sahel greening trend. Geophys. Res. Lett. 32 (21), 365–370.

Huang, J., et al., 2017a. Dryland climate change: recent progress and challenges. Rev. Geophys. 55 (3).
Huang, J., Yu, H., Dai, A., Wei, Y., Kang, L., 2017b. Drylands face potential threat under 2 °C global warming target. Nat. Clim. Chang. 7 (6).
Jarvis, P.G., L.S, 2000. Botany - Constraints to growth of boreal forests. Nature 405 (6789), 904–905.
Jung, M., et al., 2010. Recent decline in the global land evapotranspiration trend due to limited moisture supply. Nature 467 (7318), 951.
Kendall, M.G., 1955. Rank Correlation Methods.
Kurc, S.A., B.L.M, 2010. Digital image-derived greenness links deep soil moisture to carbon uptake in a creosotebush-dominated shrubland. J. Arid Environ. 74 (5), 585–594.
Lü, Y., et al., 2015. Recent ecological transitions in China: greening, browning, and influential factors. Sci. Rep. 5, 8732.
Lu, X., Wang, L., McCabe, M.F., 2016. Elevated CO_2 as a driver of global dryland greening. Sci. Rep. 6, 20716.
Mann, H.B., 1945. Nonparametric tests against trend. Econ.: J. Econ. Soc. 245–259.
Martens, B., et al., 2017. GLEAM v3: satellite-based land evaporation and root-zone soil moisture. Geosci. Model. Dev. 10 (5), 1903–1925.
McVicar, T.R., et al., 2012. Global review and synthesis of trends in observed terrestrial near-surface wind speeds: implications for evaporation. J. Hydrol. 416–417, 182–205.
Milly, P.C.D., Dunne, K.A., 2016. Potential evapotranspiration and continental drying. Nat. Clim. Chang. 6 (10).
Miralles, D., et al., 2011. Global Land-Surface Evaporation Estimated from Satellite-Based Observations.
Miralles, D.G., et al., 2014. El Niño–La Niña cycle and recent trends in continental evaporation. Nat. Clim. Chang. 4 (2), 122.
Monteith, J.L., 1965. Evaporation and environment. Symp. Soc. Exp. Biol. 19 (19), 205–234.
Mueller, N.D., et al., 2016. Cooling of US Midwest summer temperature extremes from cropland intensification. Nat. Clim. Chang. 6 (3), 317.
Nemani, R.R., et al., 2003. Climate-driven increases in global terrestrial net primary production from 1982 to 1999. Science 300 (5625), 1560–1563.
Notaro, M., L.Z, Gallimore, R.G., et al., 2010. Complex seasonal cycle of ecohydrology in the Southwest United States. J. Geophys. Res. Biogeosci. 115 (G4).
Peng, D., Zhou, T., 2017. Why was the arid and semiarid northwest China getting wetter in the recent decades? J. Geophys. Res. Atmos. 122 (17), 9060–9075.
Penman, H.L., 1948. Natural evaporation from open water, bare soil and grass. Proc. R. Soc. Lond. 193 (1032), 120.
Poulter, B., et al., 2014. Contribution of semi-arid ecosystems to interannual variability of the global carbon cycle. Nature 509 (7502), 600.
Ren, J., Liu, H., Yin, Y., He, S., 2007. Drivers of greening trend across vertically distributed biomes in temperate arid Asia. Geophys. Res. Lett. 34 (7).
Roderick, M.L., Greve, P., Farquhar, G.D., 2015. On the assessment of aridity with changes in atmospheric CO_2. Water Resour. Res. 51 (7), 5450–5463.
Scheff, J., Frierson, D.M., 2014. Scaling potential evapotranspiration with greenhouse warming. J. Clim. 27 (4), 1539–1558.
Shuttleworth, W.J., 2007. Putting the' vap' into evaporation. Hydrol. Earth Syst. Sci. 11 (1), 210–244.
Sun, S., et al., 2016. On the coupling between precipitation and potential evapotranspiration: contributions to decadal drought anomalies in the Southwest China. Clim. Dyn. 48 (11–12), 3779–3797.
Swann, A.L., Hoffman, F.M., Koven, C.D., Randerson, J.T., 2016. Plant responses to increasing CO_2 reduce estimates of climate impacts on drought severity. Proc. Natl. Acad. Sci. U. S. A. 113 (36), 10019.
Tan, Z.H., Z.Y.P, Deng, X.B., et al., 2015. Interannual and seasonal variability of water use efficiency in a tropical rainforest: results from a 9 year eddy flux time series. J. Geophys. Res. Atmos. 120 (2), 464–479.
Turnbull, L., W.J, 2019. From structure to function: understanding shrub encroachment in drylands using hydrological and sediment connectivity. Ecol. Indic. 98, 608–618.
Ulf Helldén, T.C., 2008. Regional desertification: a global synthesis. Glob. Planet. Change 64 (3–4), 0–176.
Wang, K., Dickinson, R.E., 2012. A review of global terrestrial evapotranspiration: observation, modeling, climatology, and climatic variability. Rev. Geophys. 50 (2).
Wang, X., et al., 2017. Moisture-induced greening of the South Asia over the past three decades. Glob. Chang. Biol. 23 (11), 4995–5005.
Wolf, S., et al., 2016. Warm spring reduced carbon cycle impact of the 2012 US summer drought. Proc. Natl. Acad. Sci. 113 (21), 5880–5885.
Yang, Y., S.Z, McVicar, T.R., Beck, H.E., Zhang, Y., Liu, B., 2018a. Disconnection between trends of atmospheric drying and continental runoff. Water Resour. Res. 54, 4700–4713.
Yan, J., Z.D, Liu, J., et al., 2014. Interactions between CO_2 enhancement and N addition on net primary productivity and water-use efficiency in a mesocosm with multiple subtropical tree species. Glob. Chang. Biol. 20 (7), 2230–2239.
Yang, Y., Di, L., Guan, H., Scanlon, B.R., Xiang, X., 2015. GRACE satellite observed hydrological controls on interannual and seasonal variability in surface greenness over Mainland Australia. J. Geophys. Res. Biogeosci. 119 (12), 2245–2260.
Yang, Y., L.D, Guan, H., et al., 2014. GRACE satellite observed hydrological controls on interannual and seasonal variability in surface greenness over mainland Australia. J. Geophys. Res. 119 (12), 2245–2260.
Yang, Y., Roderick, M.L., Zhang, S., McVicar, T.R., Donohue, R.J., 2018b. Hydrologic implications of vegetation response to elevated CO_2 in climate projections. Nat. Clim. Chang. 9 (1), 44–48.
Zeng, Z., et al., 2012. Global evapotranspiration over the past three decades: estimation based on the water balance equation combined with empirical models. Environ. Res. Lett. 7 (1), 014026.
Zeng, Z., et al., 2014. A worldwide analysis of spatiotemporal changes in water balance-based evapotranspiration from 1982 to 2009. J. Geophys. Res. Atmos. 119 (3), 1186–1202.
Zhu, Z., et al., 2016. Greening of the Earth and its drivers. Nat. Clim. Chang. 6 (8), 791–795.